Skull Reconstruction Using Statistical Shape Models

Patrik Rosendal

Master's thesis
2020:E37

Lund University

Faculty of Engineering
Centre for Mathematical Sciences
Mathematics

Centrum Scientiarum Mathematicarum

Skull Reconstruction Using Statistical Shape Models

Patrik Rosendal

2020–08–11

Supervisor: Einar Heiberg, Niels Christian Overgaard
Examiner: Magnus Oskarsson

Abstract

In case of a head injury or trauma a surgeon opens up the skull by removing a bone piece of the skull to either relieve pressure or get access to brain tissue. The first option is to follow up with putting back the same skull piece. In the circumstances this is not possible however, a surgeon must open up the skull and form a piece using bone cement that fits the whole during the surgery, which is time consuming This leads to an increase risk of infection and other medical risks for the patient.

This project investigates the possibility to mathematically reconstruct the piece missing in the skull, giving the surgeon the option to already have a fitted piece ready before the operation begins.

The goal of the project was to investigate if a statistical shape model could be used for cranial reconstruction. The model was built from a data set from Skåne University Hospital, it was preprocessed using Medviso Segment 3D Print software and all other implementation was done in Matlab. Each skull were sampled to a point cloud, with skull radii and thickness as parameters. The shape model was built from a point cloud sampled from each skull. The skulls were registered to each other using ICP registration. The resulting model reconstruct successfully a damaged skull with 1 mm average error. Six modes were enough to account for 90% of the shape variability. The results of average error of 1 mm was not deemed enough to be clinically useful.

Acknowledgements

I would like to thank Einar Heiberg and Niels Christian Overgaard for their work as supervisors supporting every part of this thesis. As a whole I would like to send my gratitude to the Cardiac MR Group, Medviso and their employees, Helen, Karolina and Klas among others, for giving me a place to study and work on as well as a place for social interaction and spontaneously discussions. I would also like to thank Philip Bernborg from Bild och funktion on Skåne University Hospital for giving me the time to test 3D printing of some skull parts. I would like to thank David Belfrage for his engagement in the project concerning computational efficiency of certain geometric applications.

Contents

1 Introduction

1.1 Background

In circumstance of a head wound, stroke, tumour or malformations in the skull sometimes a piece of the skull bone has to be removed either to relieve pressure or to get access to brain tissue. In many of these events the first option is to put back the skull piece removed when the surgery has been carried out. However sometimes the bone piece is itself infected or defected making it unsuitable or making it a high risk for complications when putting the bone piece back in. For these cases cranial reconstruction surgery is needed, reconstructing the bone part missing and surgically put it into place.

When a damaged cranium is in need of surgical reconstruction different techniques are used. These techniques require that the surgeon open up the skull and then relying on their own ability to craft and mould a piece using bone cement that fits the cranial hole during one procedure.

Another situation where reconstruction of the skull could be beneficial is when the skull for various reasons malformed and part of the skull is to be removed. In a case such as this, providing a cutting guide for the surgeon of what part of the bone to be removed, could be beneficial.

The biggest disadvantage with the current methods is that the skull is laying open for a long time which leaves the patient susceptible to an infection and other complications. If the piece that patches the skull together is known before the skull is being opened, that part could be manufactured before the surgery, leading to a faster surgery with less chance of infection and complications for the patient.

One of the key advancements in recent years that can make the method proposed in this report viable, is that of 3D-printing custom made parts. Being able to 3D-print locally a given shape brings down both cost and time to manufacture. While methods of 3D-printing where the parts can actually be inserted into the body is not yet available to hospitals, there are 3D-printers which can 3D-print plastic of which can be in contact (after decontamination) with material that is then to be inserted into the body. That is a mould can be 3D-printed, decontaminated and then used to mould the piece that is to be inserted into the patients head.

At the neurosurgical clinic at Skåne University Hospital there is made about 1000 cranial surgeries per year where the skull is opened. In about 5% of these cases there is no bone to put back, mainly because of infections or risk of infections in the previously removed bone parts. In those cases bone cement is manually formed to fit the skull hole and for these patients a method in which a fitted bone part have been made ready before the operational procedure has

begun would be beneficial not only for the patients but for the hospital as well.

Medviso AB in collaboration with Skåne University Hospital is doing a research project on skull and wrist bone reconstruction for surgical application using machine learning. This is part of a bigger research initiative on the Analytic Imaging Diagnostics Arena (AIDA) platform where researches within the field of AI and the medical clinical make cross-discipline collaborative research.

1.2 Project Objective

The goal is to build a theoretical model that successfully reconstructs a defect cranium where the defect could be a hole in the skull or any other shape that is common in current cranial reconstructing surgery. Because of the simpler geometry of the cranial part than that of the face part of the skull the project is limited to only cranial reconstruction.

1.3 Approach

To solve this problem a statistical shape model will be constructed of the human skull. The idea is to fix a point at the centroid of the cranium and from this point the cranium will be sampled in both longitude and latitude angles. Further a shape model will be constructed and using principal component analysis (PCA) a basis for the cranium can be found. A skull can then be reconstructed by projecting it to this basis. For this method to be successful many samples of human skulls needs to be collected.

Part of the project will be to investigate skull shape surface variation and how many skulls is required for statistical shape representation for any given skull.

2 Theory

This chapter introduces the concepts of Principal Component Analysis, Iterative Closest Point Registration and Statistical Shape Models.

2.1 Principal Component Analysis

Principal Component Analysis (PCA) is a statistical method used on a large set of correlated variables and produces through a linear transformation a smaller set of uncorrelated, or orthogonal, variables. The principal components are ordered such that the first component contains the largest variation in the data set and each following component, under the constraint of being orthogonal to all previous components, contains as much variation as possible in the data set.

To perform PCA on a data set with m samples of dimension n they are placed in a $m \times n$ matrix $\mathbf{X}$ with m rows and n columns, that is each row represents a sample and each column represents a dimension of the data set. The average of all samples is formed,

$$\bar{\mathbf{X}} = \frac{1}{m} \sum_{i=1}^{m} \mathbf{X}_i, \tag{1}$$

which is then subtracted from each samples in $\mathbf{X}$

$$\tilde{\mathbf{X}} = \mathbf{X} - \bar{\mathbf{X}}. \tag{2}$$

The covariance matrix is formed of the zero mean data matrix ,

$$\mathbf{C} = \frac{1}{m} \tilde{\mathbf{X}}^{\intercal} \tilde{\mathbf{X}}. \tag{3}$$

Calculating the eigenvectors of the covariance matrix satisfies,

$$\lambda_i \mathbf{V}_i = \mathbf{C}\mathbf{V}_i, \tag{4}$$

where there are $i = 1, \ldots, n$ eigenvalues with corresponding eigenvectors. The eigenvalues satisfies the condition of $\lambda_i > \lambda_{i+1}$ and each eigenvector $\mathbf{V}_i$ corresponds to a principal component.

The PCA method is based on the assumption that variation in the data set implies information in the data set. This means that biases that gives higher variation for certain dimensions has to removed before PCA is being applied [5].

2.2 Iterative Closest Points Registration

Iterative Closest Points Registration (ICP) [4] is a method to align two partially overlapping shapes using a rigid transformation. The method works iterative and can be used on many different data types, for this report we are going to consider two point clouds where one should be registered to the other. The ICP

registration algorithm can be summed up as:

0. Rough alignment between moving and fixed shapes.
1. Find corresponding points between moving and fixed shapes.
2. Align corresponding points.
3. Calculate alignment error of all points that found correspondence.
4. Repeat 1-2-3 until threshold on error or number of iterations is reached.

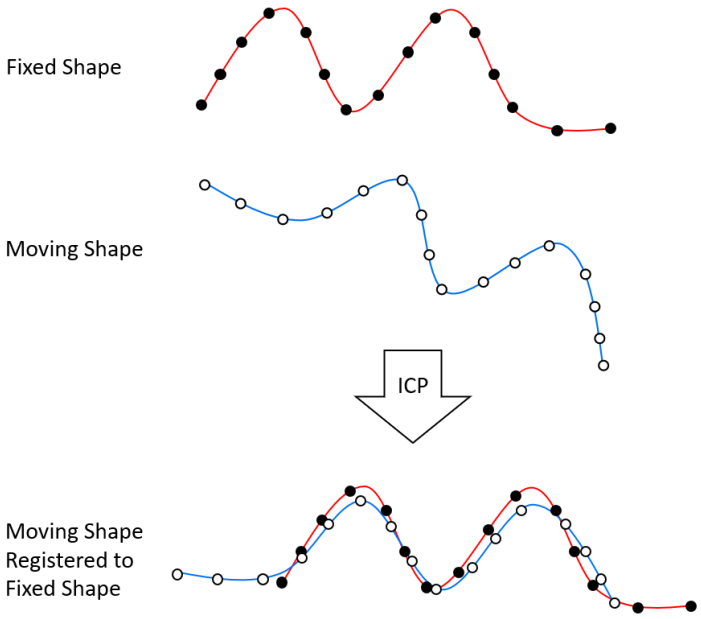

Figure 1: Illustration of ICP Registration.

Consider a set of moving points X and a set of fixed points Y, to register X to Y an initial alignment is done first. The set of points in X and Y are ordered in the matrices $\mathbf{X}$ and $\mathbf{Y}$, where each row in respective matrix corresponds to a point in respective set of points.

The initial rough alignment of the shapes is done by finding the best scale, rotation and translation, by minimising;

$$\min_{s,\mathbf{R},\mathbf{t}} ||\mathbf{Y} - s\mathbf{R}\mathbf{X} + \mathbf{t}||, \tag{5}$$

Correspondence can be found using any method of choice, for example matching landmark points. For this thesis finding correspondence between points were chosen as the closest points to another in the two sets, that is the point x_i in

the set of moving points X corresponds to y_j in the set of fixed points Y;

$$j = \arg \min_{k=1,\ldots,n} d(x_i, y_k), x_i \in X, y_k \in Y \tag{6}$$

where $d(x, y)$ is the Euclidean distance between the two points x and y.

Alignment is done using only the subset of points in the data set that has found a correspondence, in the case of using nearest point as correspondence all points in the moving set will find a corresponding point on the fixed set, though not all points on the fixed set might have a point from the moving set corresponding to them. Alignment is done by minimising the error using scaling, rotation and translation the same way initial rough alignment was done, though only using the points that has found correspondence.

The procedure continues iterative until the alignment error, calculated using RMS on corresponding points, is small enough or it has been iterated the number of times set as upper bound as number of iterations or a combination of both.

2.3 Statistical Shape Models

A statistical shape model is an analytic tool geometrical properties of shapes. The shape model uses some parameterization for the shape and models this shapes variation through the use of statistical methods. For this project the focus is on using PCA on a shape represented by a points cloud to model the shape variation. Alignment or registration techniques is also commonly used. A limitation of the shape model using PCA is that it can only represent shapes within the linear space that the data set represent.

For the shape analysis in this report the following procedures was used:

Let $\mathbf{X}_i$, $i = 1...n$, be n number of shapes. Where $\mathbf{X}_i$ is a vector representing a point cloud of our given shape. Align the shapes to one another, rigid or non rigid methods, for example using Procrustes analysis. Calculate the mean value of all shapes, $\bar{\mathbf{X}} = \frac{1}{n}\sum_{i=1}^{n} \mathbf{X}_i$, and subtract the mean from each shape, $\tilde{\mathbf{X}}_i = \mathbf{X}_i - \bar{\mathbf{X}}$. Do PCA on the set $\{\tilde{\mathbf{X}}_i, i = 1...n\}$, calculate the covariance matrix $\mathbf{C} = \frac{1}{n}\tilde{\mathbf{X}}^\intercal\tilde{\mathbf{X}}$ and solve for eigenvalue and eigenvectors $\lambda_j\mathbf{V}_j = \mathbf{V}_j\mathbf{C}$. The eigenvectors $\mathbf{V}_j$, $j = 1...m$ are the modes in our shape model where the eigenvalues λ_j represents significance of variation in corresponding mode $\mathbf{V}_j$.

The set of our eigenvectors or modes $\mathbf{V}_j$ is a basis for where we can project new shapes. Where the representation of a new shape $\mathbf{S}$ in this shape model will can be formed by $\hat{\mathbf{S}} = \bar{\mathbf{X}} + \mathbf{V}(\mathbf{S} - \bar{\mathbf{X}})$ which will be the closest approximation of $\mathbf{S}$, that minimises the quadratic error, in this linear space that the basis $\mathbf{V}$ spans [6].

3 Materials and Methods

3.1 Data

The skulls come in the Digital Imaging and Communications in Medicine (DICOM) file format. DICOM is a standardised medical imaging file format used world wide. The DICOM file format contains in addition to the scanning data of the skull also information of the person scanned, device information etc. For this project, the persons were deidentified, removing some of the otherwise available information. The information used in this study was the CT slices of the skull and information about resolution and slice thickness.

3.1.1 Data from Skåne University Hospital

The data was collected came from CT scans of the skulls at the Skåne University Hospital. A total of 30 skulls were provided for the study. The skulls were from patients already undergoing CT scans used for clinical investigation and ethical permission was waived by ethics committee (Dnr 2019-02264) provided that complete and irreversible anonymisation was performed prior to analysis.

Age span and gender of the persons in the data are unknown. And since the data is anonymized no other information of how good the data represents the general population is known. Because of the anonymisation knowledge about the data sets skewness remains unknown. While precautions can be made against having a too small data set by adding more skulls, not knowing how well they represent the general population would still remain an issue.

Spatial Resolution [mm]

x	y	z
0.4297	0.4297	0.5000

3.1.2 Data from The Cancer Imaging Archive

In order to get access to more data for the shape model other sources for data were investigated. One place to find medical data is The Cancer Imaging Archive (TCIA) which is an open source image archive of many types of medical images. One type of the images stored is CT scans of patients with cancer in the neck, throat or head. The data for this type of cancer often provided with CT scans of the whole cranium which is what desired for this project. A number of 500 CT scans of neck, throat or cancer in the head was found. However after initial investigation it was found that the spatial resolution of the relevant CT scans found at TCIA was too low with a spatial resolution below 1 mm, in some directions the resolution was as bad as 3 mm, as seen in Figure 2 which considering the skull bone thickness varying from 3-14 mm [1] is far too low with the current approach.

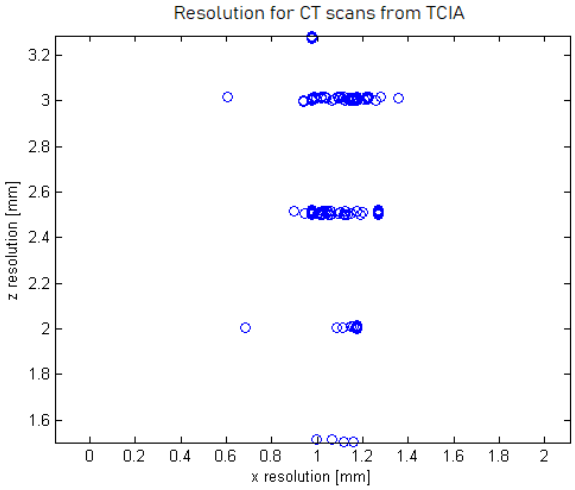

Figure 2: The spatial resolution for the CT images found at the TCIA data base. Each dot represents the x and z resolution for a single CT scan of the head.

3.2 Software

For screening the data, Segment 3D Print was used. Segment 3D Print is a Matlab based medical imaging software developed by Medviso AB. The software reads DICOM files that can be looked at which allowed for screening the data. Segment 3D Print also made it possible to make some simple but effective preprocessing; segmentation, cropping, smoothing among other features. Finally Segment 3D Print also made it possible to extract a file of the skull that could be analysed by user made tools in the Matlab environment.

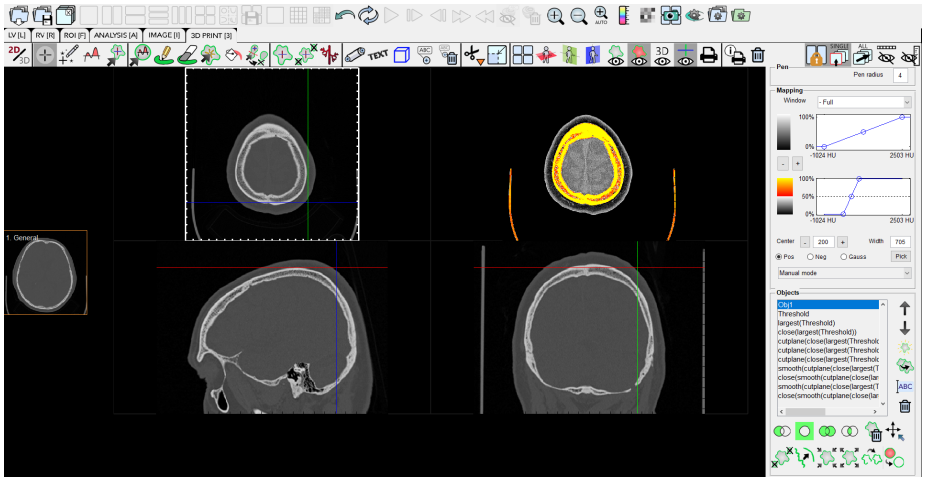

Figure 3: Overview of the Segment 3D Print interface.

The Matlab environment was used to do the programming and analysis of the data. The Matlab 2018b version was used. Matlab 2018b had support for some mathematical packages and graphical features not present in earlier version. Some open source packages supporting efficient computation was used to reduce processing time.

3.3 Hardware

A computer with the following specification were used for the computational workload.

CPU	Intel i7-6700HQ
RAM	16 GB DDR4
GPU	GeForce GTX 960M

3.4 Algorithm

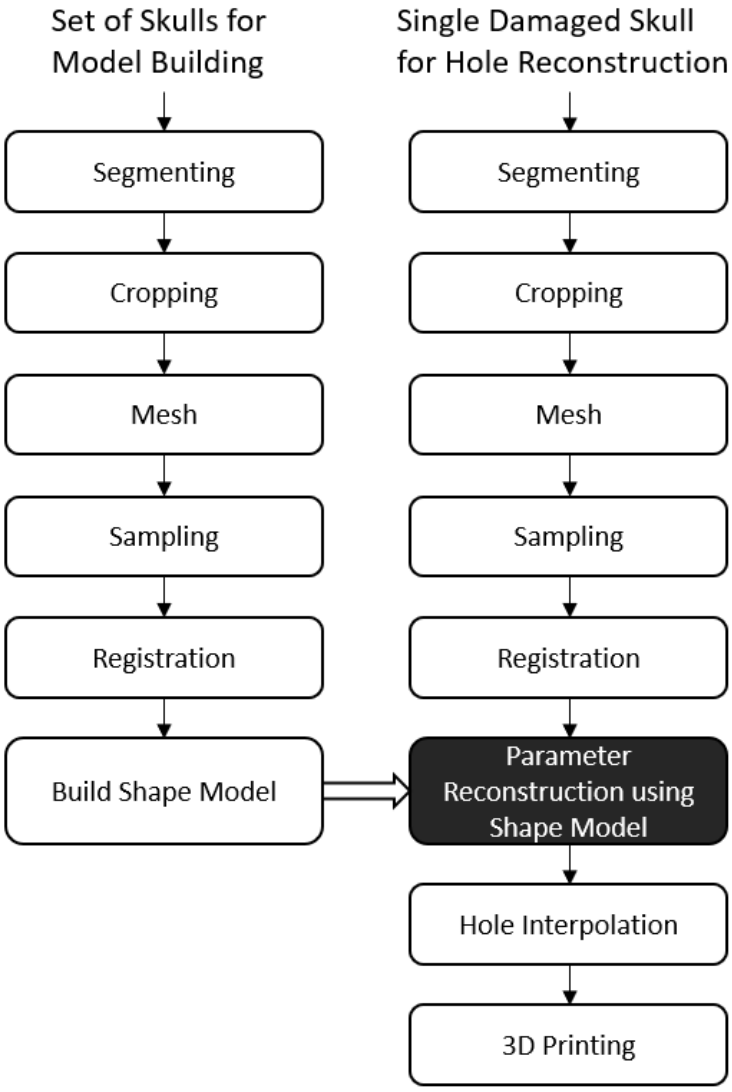

Figure 4: An overview of the algorithm flow chart. To the left the flow chart for building the shape model. To the right the flow chart to reconstruct a hole of a skull.

3.5 Screening

A necessary condition for the skull to be part of the statistical model were that all parts of the cranium were intact and no parts were missing. No holes or defects were allowed and the whole skull had to be part of what was scanned. The motivation for this criteria is that the PCA builds up a statistical model using the covariance of the whole data set, if there is missing values for a part of the data set no covariance can be calculated.

A spatial resolution of at least 1 mm was initially determined necessary for the skull to be considered of high enough resolution for it to be part of the model. This was motivated by if the spatial resolution of the scan was too low the resulting CT scan sometimes failed to pick up thin bone parts, especially the forehead was sensitive because of the sinus cavities inside the bone at the forehead. This was the case for many of the skulls in the TCIA data set mentioned earlier. Further a high resolution was motivated by that you need data of a high resolution if you want to measure the error of high resolution.

Because of practical implementation restriction all skulls had to be roughly oriented in the same direction.

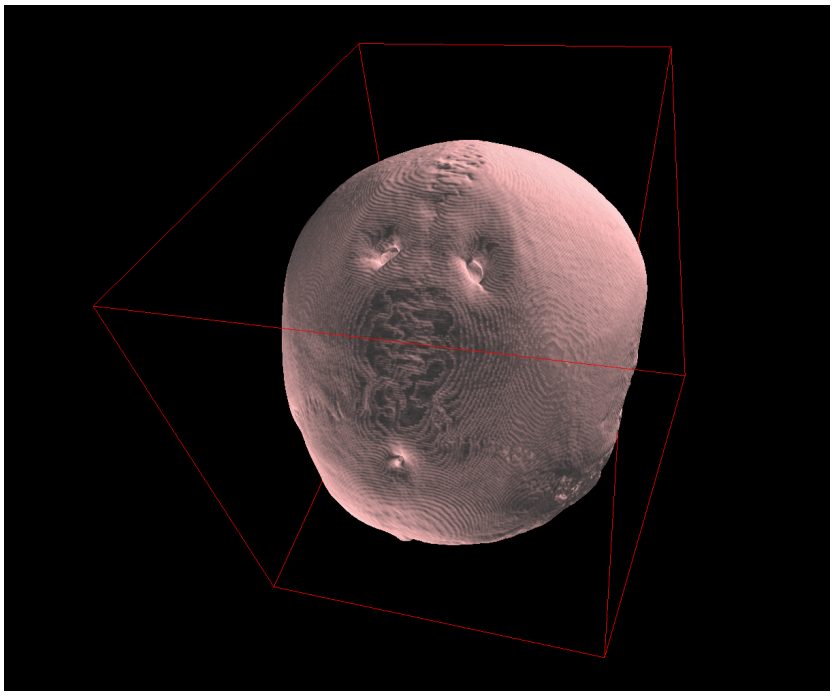

Figure 5: An example of a defective skull that was manually removed from the data set while screening. Three smaller holes in the back of the head would have made the PCA incomplete.

3.6 Preprocessing, segmentation, cropping

The CT scans contains radiodensity, measured in the unit of Hounsfield [HU], for each voxel. Different parts of the human body has different attenuation which makes it possible to see the morphology of different organs, tissues or fluids in the human body. An example of a CT scanned human skull is shown in Figure 6.

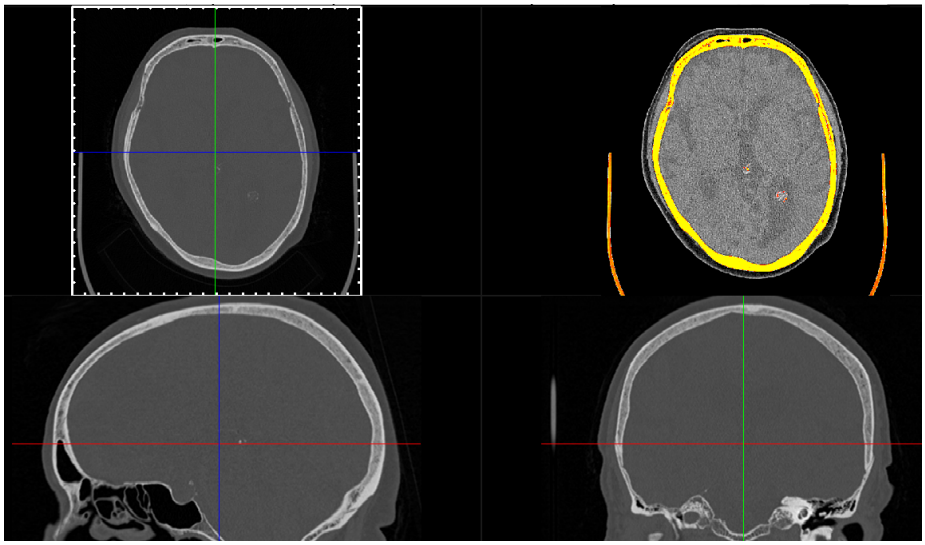

Figure 6: Unsegmented skull, selected slices preview. Top left - transervsal slice, bottom left - sagittal slice, bottom right - coronal slice, top right - segment preview

Because bone has higher attenuation than other human tissue in general segmentation of the cranium can be done with a simple threshold, that is all voxels with data for attenuation within a certain interval is to be considered bone. The interval chosen for radiodensity is $800 - 2000$ HU. In Figure 7 the result of the segmentation is shown.

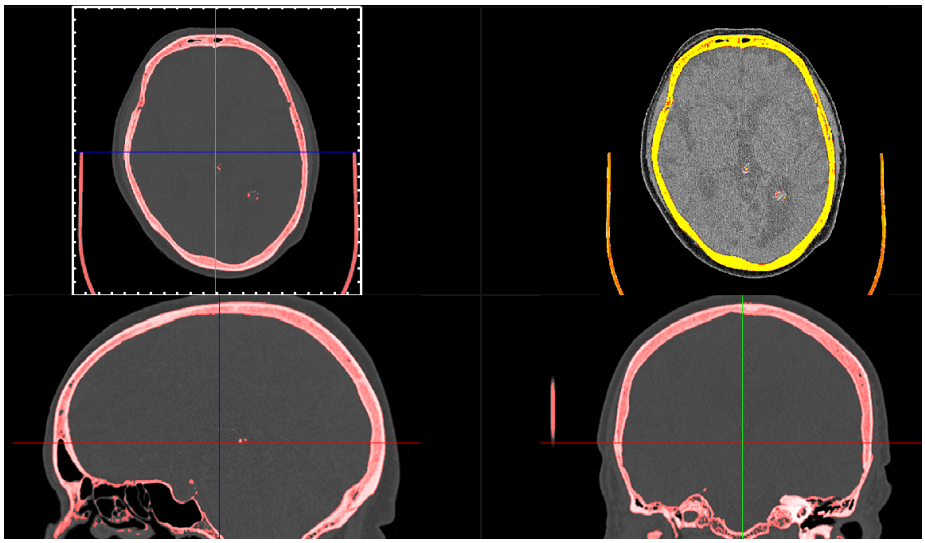

Figure 7: Segmented skull with threshold, selected slices. Red/pink colour corresponds to segmented parts of the skull made of bone.

One problem with the segmentation of the cranium was that it also picks up other non human material, this can be seen in Figure 8. These non bone parts picked up by the threshold was removed using software tools that enables objects non touching objects to be sorted by size, since the cranium always was the biggest segmented object it was selected to be kept while other segmented objects where removed. In Figure 7 there is visible segmented bone parts, in the middle of the skull of the transversal and sagittal slice, that could later disturb the sampling of the skull. These unwanted segmented bone parts had to be removed as well and it could be done using the same "choose largest object" tools as mentioned previously.

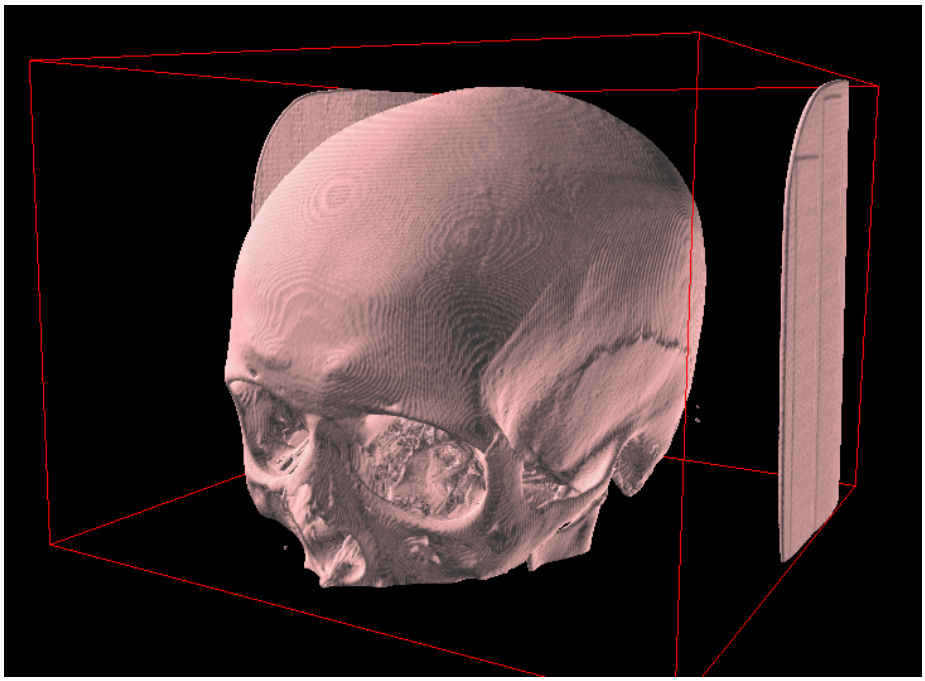

Figure 8: Segmented skull with threshold, viewed with 3D viewer.

Another software feature used to get a desirable result were a filling out cavities feature, this was however mostly done to simplify the geometry for computations done later in the program and it didn't have an impact on the final statistical model.

The craniums were, after proper segmentation, cropped with a transversal crop in such a manner that the complicated geometry that the face and lower half of a human skull contains were removed. To ensure that the cut was consistently made at the same place for all skulls a landmark was chosen as where the zygomatic bone connects to the frontal bone at the forehead, also known as the temple, this can be seen in Figure 9. The landmark was clearly seen in the 2D slice viewer, as well with how other desirable or undesirable parts of the skull would be included or excluded from the selected crop. The annotation of the landmark was done by the student himself.

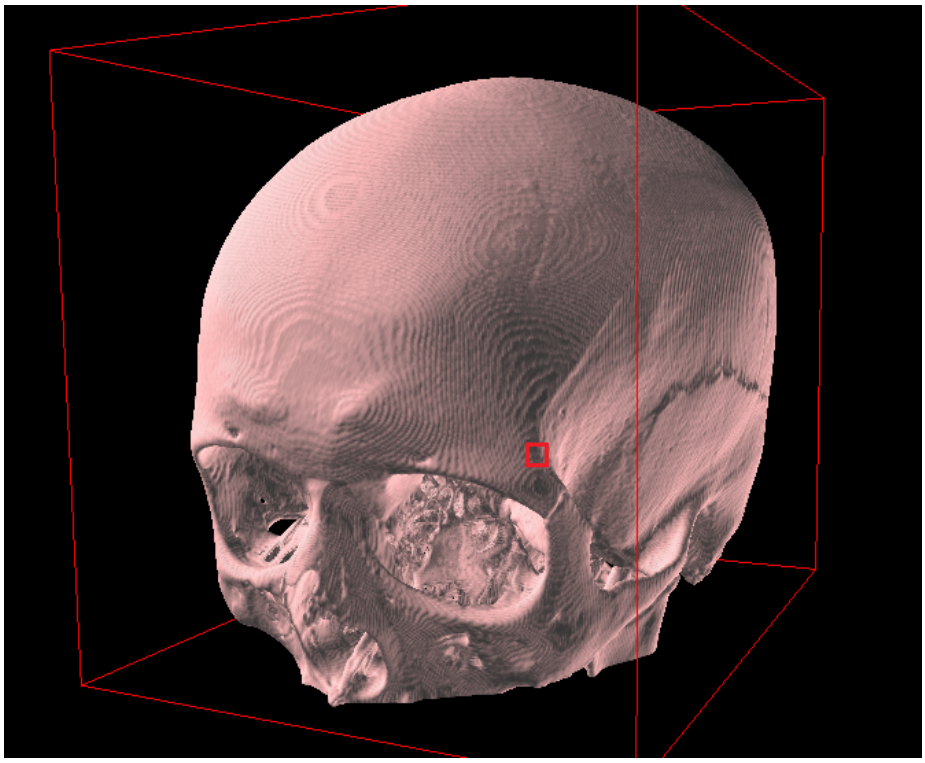

Figure 9: Chosen landmark for transversal crop marked with red square at the zygomatic bone.

The result of the skull being segmented and cropped can be seen in Figures 10, 11 and 12. A comparison can be done with Figure 10 and Figure 7.

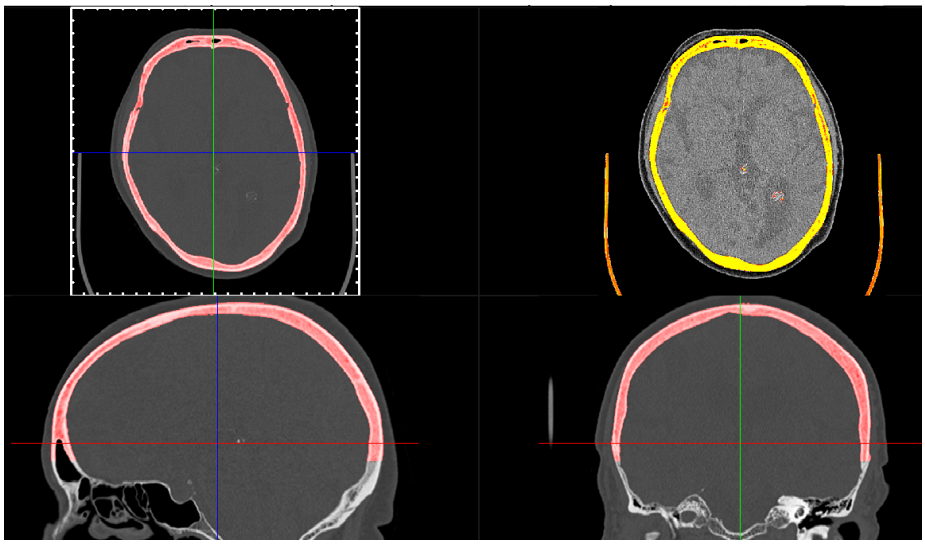

Figure 10: Cropped skull with threshold, viewed in selected slices.

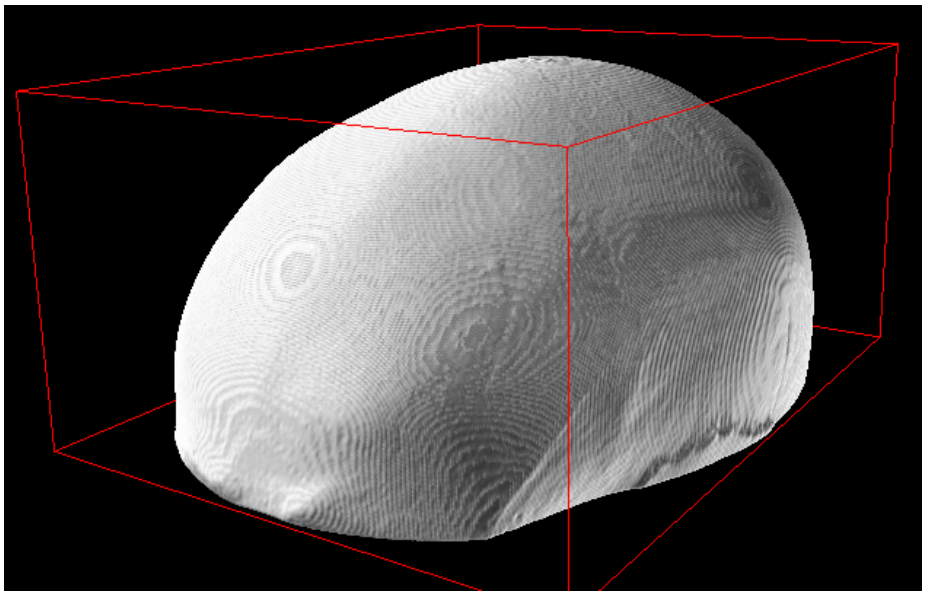

Figure 11: Cropped skull, viewed with 3D viewer.

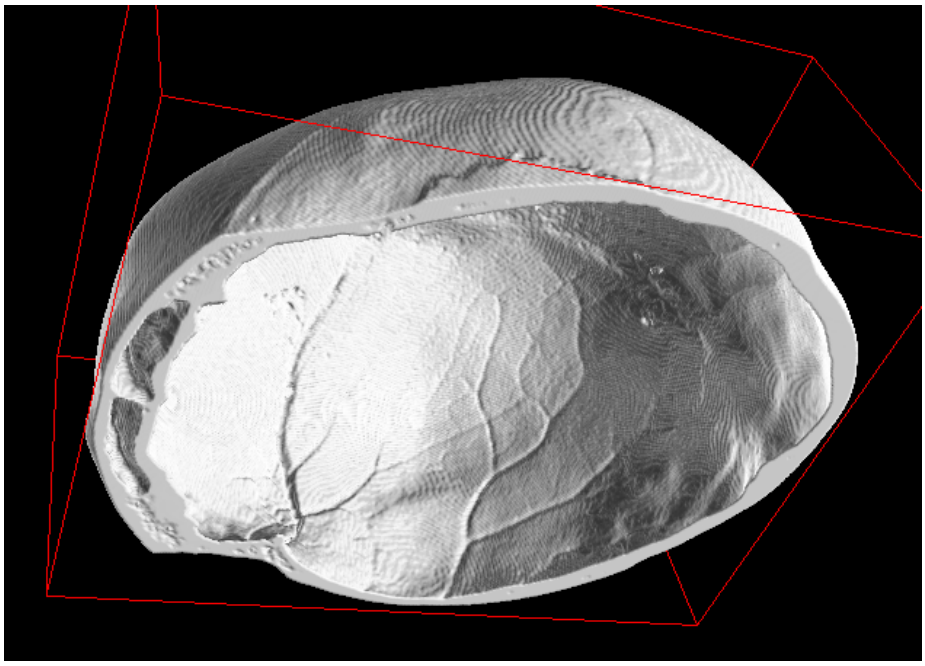

Figure 12: Cropped skull, viewed from below with 3D viewer.

3.7 Making Holes

For each skull four damaged skulls were created for the purpose of testing the skull reconstruction algorithm. The holes were placed on the front, back and both sides of the upper part of the skull. The size of the holes were about 3×2 cm.

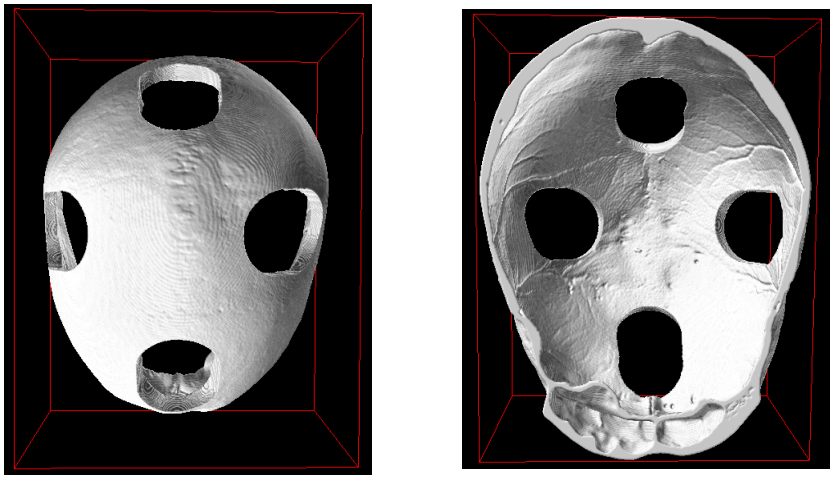

(a) Top view.

(b) Bottom view.

Figure 13: Example of holes generated to create test data. Here all holes are shown on a single skull for the purpose of presentation, in the project they were all done on a different skull copy.

3.8 Mesh

The segmented and cropped skull, both with and without holes, in the format of a 3D voxels containing data about the presence of bone within it, was converted to a triangular mesh where the outer wall of the mesh approximated the outer wall of the cranium and the inner wall of the mesh approximated the inner wall of the cranium. This allowed for measuring of distance between the inner and outer wall of the skull, which was used in the parameterization of the skull.

3.9 Skull Sampling

The skulls were sampled to a points cloud to build up the shape model. The skull triangular mesh was sampled using rays shooting out from a centre point chosen by the user. The rays were chosen such that it sampled a sphere evenly along the surface. An assumption was made regarding the shape of the skull cranium that is quite spherical and therefore a good sampling of a sphere would imply a good sampling of a skull. The sampling was done with about 2000 points.

Initially, an idea was to create the set of rays used for sampling by creating a grid in the polar coordinate system and then transform that to the Cartesian coordinate system. The advantage of this method would have been that it would be simple to implement and there would for each ray have been a clear neighbouring ray along the latitude and longitude axis, a property that might have been proven useful. This method was ultimately discarded because of the skewness it introduced to distribution of the sampled points.

The chosen sampling method used was instead to sample a half sphere in layers, where each layer was separated by a fixed arc length and where the number of sample point in each layer was approximated to the circumference divided by this arc length. Given that no perfect sample method of the sphere exists where the sampled points is equidistant, this method was considered good enough for the purpose of this project. In Figure 14, a sampled half sphere with this method is shown.

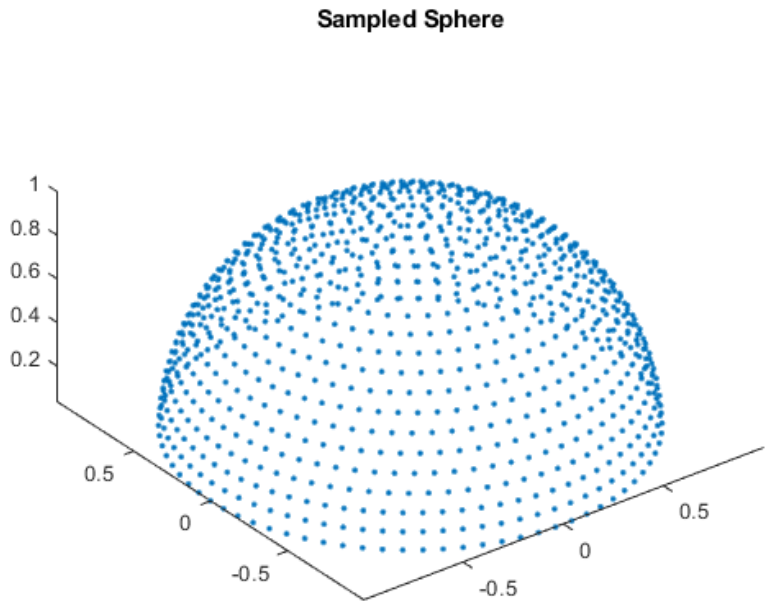

Figure 14: Sphere sampled with rays ordered in layers. The rays intersection points are spread out evenly on the sphere

To sample the skull a point of centre of where the rays would start had to be chosen. Different methods were considered, to use the centre of mass of the skull or to fit a sphere to the skull, ultimately the method chosen was to take

the point of the skull and project it down to the transversal plane used to crop the skull. An example of a skull sampled with rays using the method described can be found in Figure 15.

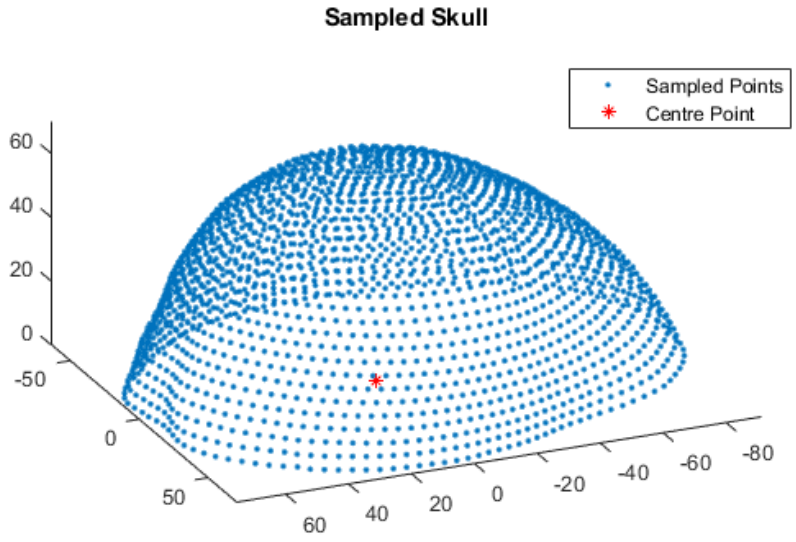

Figure 15: An example of a sampled skull. Every point represents the average of where the inner and the outer skull wall was penetrated by a ray.

The skull was sampled by a ray, represented by the point on the half sphere with the same centre, shot out from the chosen centre point of the skull and penetrating the inner and outer wall of the skull cranium. For each sampled point on the skull three properties were saved, the index of the ray, the distance from the centre point to the point in the middle of the outer and inner skull wall and the thickness of the skull wall.

3.10 Registration

Initially it was thought no registration were to be needed, since the skulls were already aligned in roughly the same orientation in the data set. It was also investigated if the shape model would model any misalignment and solve it. Even if it was possible to make it work without registration it was decided that registration could improve the result. Using registration motivates that we can be sure each point on the skull corresponds to each other, and not only relying on a guess that our naive sampling is good enough to get point to point

correspondence correct. The purpose of registration was thus both to match correspondences between data points and to strengthen our model with mathematically motivated methods.

To get something to register against an average skull was calculated. This skull had to be calculated using the naive assumption that each skull index point corresponds to each other in each skull. This proved to give a good enough average skull to have something to register towards.

When registering correspondences of two points, for example point x_i on the average skull and point y_j on the skull which we are to register, they were considered to correspond to each other if and only if x_i is the closest point among all points on the average skull to y_j and y_j is the closest point among all points on the skull to registered to x_i. This creates a problem however where there is a high likelyhood that at least some points on each skull doesn't correspond to any point on the average skull, this is because the average skull and the skulls we wish to register consist of the same amount of points and even given that they are of a similar shape its unlikely to get a one to one match for every point in the data set. To solve this problem the skulls were densely sampled while keeping the average skull as an average of the sparsely sampled skulls. This created a situation that while every point on the skull won't find a corresponding point on the average skull, each point on the average skull is very likely to find a corresponding point on the skulls to be registered.

The registration was done using Iterative Closest Point Registration (ICP). The whole registration procedure can be summarised as:

1. Calculate average skull of sparsely sampled skull.
2. Register densely sampled skulls to the average skull using ICP.
3. Find correspondences from registered skull to average skull.

One problem that couldn't be circumvented was that for certain skull no points were matching the criteria for correspondence at the edge of the skulls. This was because when the skull were registered the skull were tilted or aligned such that there were no overlapping area for that part of the skull. This created a problem that if one desired to have a complete data set these points had to removed from the model. The points removed from the model is illustrated in Figure 16.

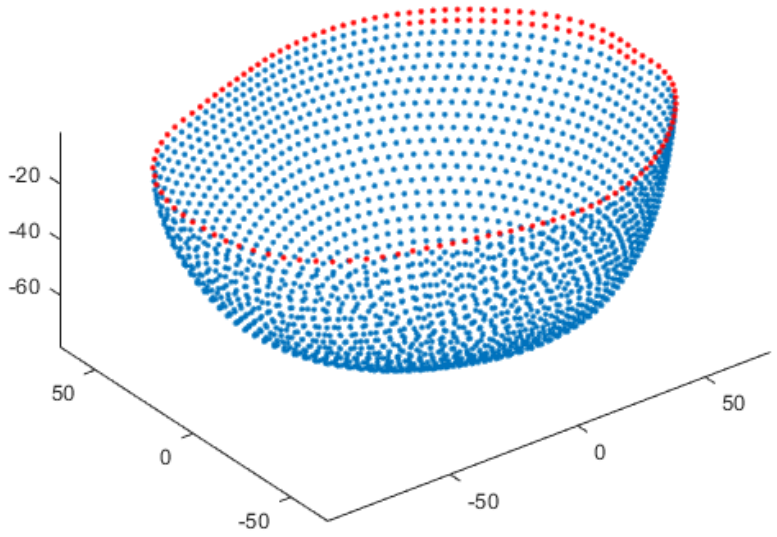

Figure 16: Points removed from the model because no correspondences could be registered for every skull in the data set. The skull is shown upside down.

3.11 Shape Model

To construct the shape model the registered point cloud was used for each skull. Because of the relative few skulls available, the shape model was built using the leave one out method. That is the shape model was constructed using every skull in the data set except the one skull we want to reconstruct. Since all skulls had multiple copies of themselves with manual holes added, the number of shape models were the same as the number of skulls.

The data was normalised so that for all skulls being part of the data set building the shape model, the average variance over skull radii and thickness parameters respectively was equal to one another. The mean skull of this normalised data set was subtracted and PCA was performed as specified in theory section.

3.12 Parameter Reconstruction

The damaged skull has an incomplete set of points in their point cloud representation, $\mathbf{x}$. First we have to remove the average skull from the damaged skull

$$\bar{\mathbf{x}} = \mathbf{x} - \bar{\mathbf{X}}, \tag{7}$$

where $\bar{\mathbf{X}}$ is the average skull used for the shape model. Projecting it on the basis the shape model creates will reconstruct an estimate the missing points. The projection can be solved by minimising:

$$\min_{\mu} ||\bar{\mathbf{x}} - \mathbf{V}\mu||, \tag{8}$$

where $\mathbf{V}$ is the basis from our shape model, $\bar{\mathbf{x}}$ is the parameters for our damaged skull vector and μ is the coefficients we want to solve for so that $\mathbf{V}\mu$ forms the least square projection of $\bar{\mathbf{x}}$ on the basis $\mathbf{V}$.

In the skull vector $\bar{\mathbf{x}}$ we got missing values representing parameters where there is a hole, where no value from radii or thickness could be retrieved in the sampling. This must first be addressed before the least square projection can be solved. Let $\{I\}$ form the set of indexes where we got missing values in $\bar{\mathbf{x}}$ and remove every column in $\bar{\mathbf{x}}$ and $\mathbf{V}$ with an index in I. Forming the new skull vector $\tilde{\mathbf{x}}$ and basis $\tilde{\mathbf{V}}$. This let's us solve the least square only for those parameters in our model where we got sampled values in $\bar{\mathbf{x}}$.

The reduced least squares projection can now be formulated,

$$\min_{\mu} ||\tilde{\mathbf{x}} - \tilde{\mathbf{V}}\mu||. \tag{9}$$

We solve it by forming the Moore-Penrose inverse,

$$\mu = (\tilde{\mathbf{V}}^T\tilde{\mathbf{V}})^{-1}\tilde{\mathbf{V}}^T\tilde{\mathbf{x}}, \tag{10}$$

and solves for our coefficients μ. In practise this was solved using the Matlab backslash operator "\", which is both more computationally and numerically efficient.

We can form the projection by multiplying with our complete basis $\mathbf{V}$ and adding our mean skull $\bar{\mathbf{X}}$, thus forming the estimate $\hat{\mathbf{x}}$ of $\mathbf{x}$,

$$\hat{\mathbf{x}} = \bar{\mathbf{V}} + \mathbf{X}\mu. \tag{11}$$

$\hat{\mathbf{x}}$ represents an estimate of the damaged skull. To get the parameters just for the reconstructed hole area those columns with index in I of $\hat{\mathbf{x}}$ is retrieved.

3.13 Hole Interpolation

The shape model gives the radii and thickness for points in an sparse grid representing the reconstructed area of the skull. Which needs to be transformed to a 3D voxel object. The parameters for the hole was converted from radii and thickness to inner and outer bone wall intersection point. The two points were transformed from the Cartesian to the polar coordinate system and a linear interpolation was done in this space. It was done in the polar coordinate system because this results in a more natural curvature for the interpolated hole.

The interpolation made the sparse parameters to a dense set of points representing the start and end of the inner and outer skull wall respectively. The voxels between these set of points where then considered to be bone.

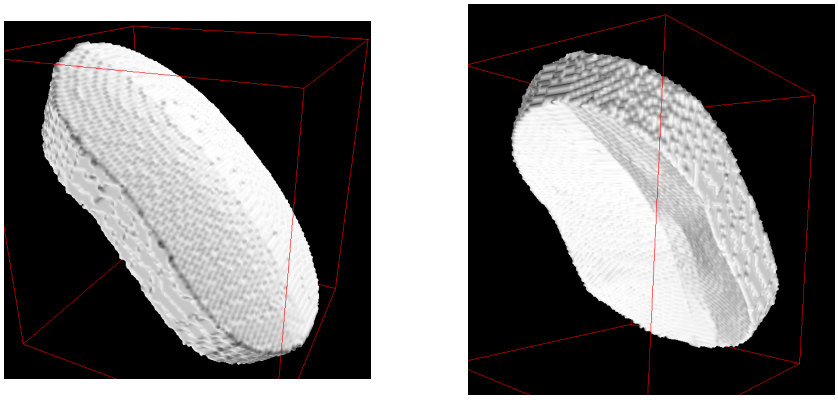

Figure 17: Example of an hole interpolation converted to 3D voxels.

3.14 3D printing

A skull with manually made holes along with the skulls interpolated holes were 3D printed. This was important to get a visual and physical feedback on the success of the hole interpolation to discuss where it was lacking or succeeding in quality. The 3D printing was done at the Skåne University Hospital with a 3D Raise Pro 3D printer.

4 Results

The two tasks of the project were to study both the shape variability and reconstruction techniques for the human skull. The results concerning shape variability is shown by looking at the variability and correlation of the parameters of the skulls used in the data set. The reconstruction result was based on the performance on how good the shape model was to reconstruct the missing parameters of the holes made on each skull.

4.1 Shape variability

The modes for the different shape models became very similar, as evident in the Figure 18. Since leave-one-out-method was used to get the most of the data set, the difference between the data sets for each shape model is just one data set. It is also clear that a few modes, about six of them, makes up more than 90% of the variability.

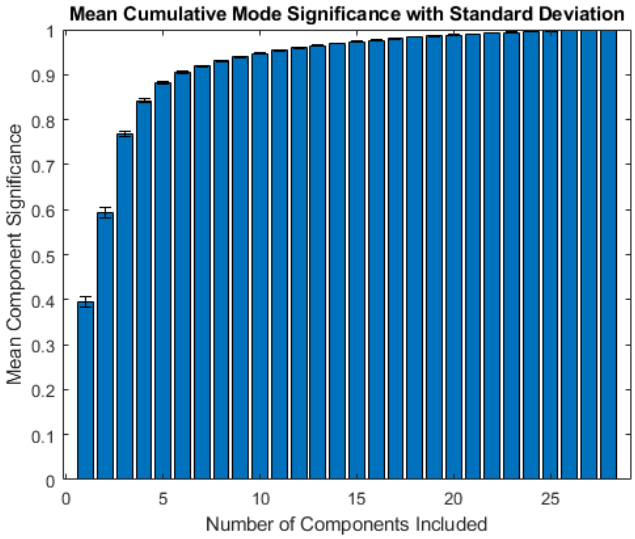

Figure 18: Mean cumulative significance for the modes in the shape models with bars showing standard deviation.

The covariance matrix, Figure 19, for the shape models can give us some insight on how different parameters is correlated. The covariance is stronger for radii parameters, also remember that the data set was normalised so that the average variance for radii and thickness parameters were the same.

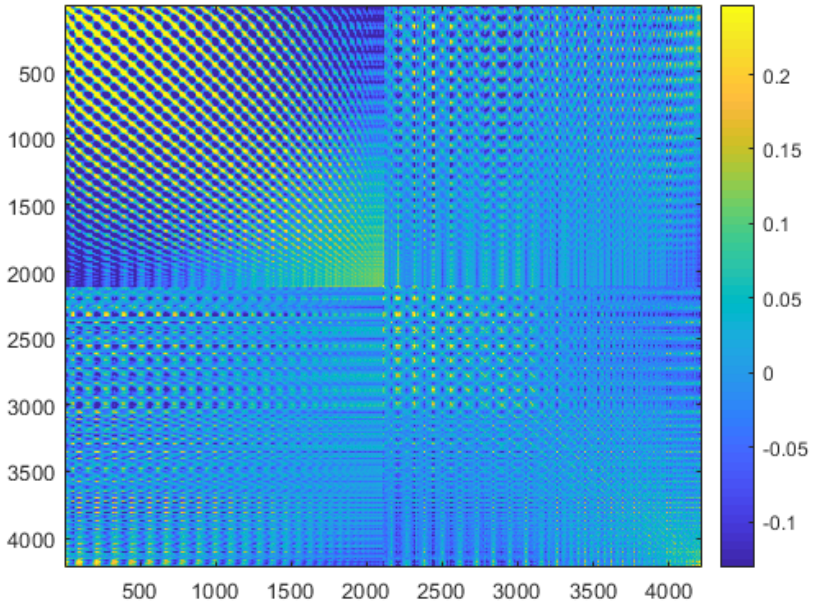

Figure 19: Covariance matrix for shape model. Top left quadrant; radial parameters covariance, bottom right quadrant; thickness parameters covariance. Top right and bottom left quadrants, radii to thickness and thickness to radii covariance.

To showcase a number of results in this report a projection of the result on the skull will be shown. This is done by taking the contour of the average skull as seen from above and then projecting the result of each parameter on that skull. This is one as to get a feeling for which parts of the skull that got affected and not only reference no parameter indexes.

The correlation is projected on the average skull. In Figure 20 and 21 the correlation between a radii parameter on the forehead and the back of the head respectively have been projected on a skull. The radii has high positive correlation locally around the parameter position and negative correlation with parameters on the opposite side of the head.

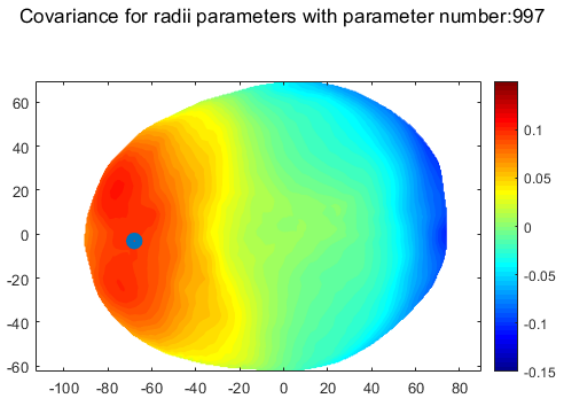

Figure 20: Covariance for radii parameter number 997 (marked with a blue dot), with other radii parameters projected on the skull.

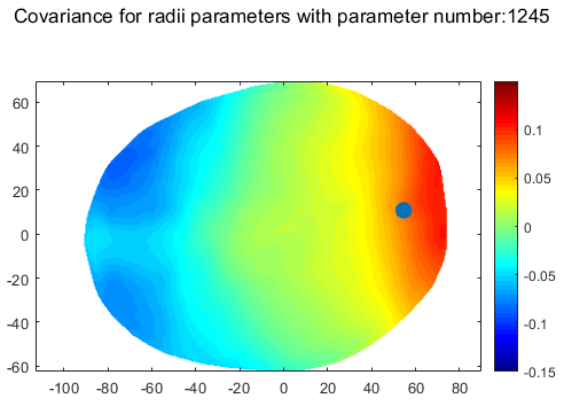

Figure 21: Covariance for radii parameter number 1245 on the forehead (marked with a blue dot), with other radii parameters projected on the skull.

The correlation for thickness parameters was also projected on a skull, see Figures 22 and 23. It is evident that the correlation is weaker overall, but there is some structure locally around the parameter.

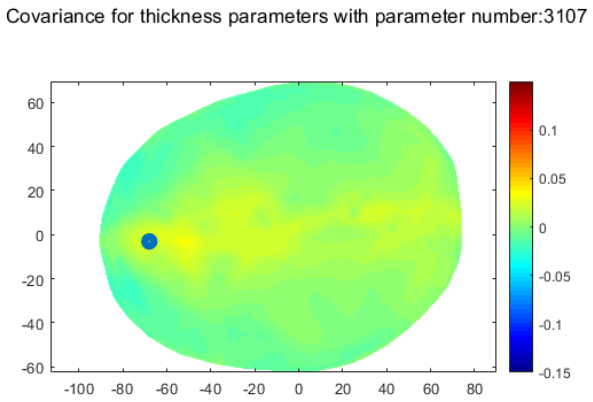

Figure 22: Covariance for thickness parameter number 3107 on the back of the head (marked with a blue dot), with other thickness parameters projected on the skull.

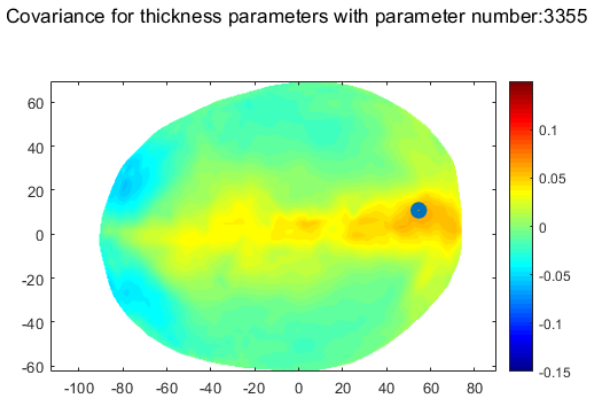

Figure 23: Covariance for thickness parameter number 3355 (marked with a blue dot), with other thickness parameters projected on the skull.

In figures 24 and 25 the correlation for a parameter on the side of the head is shown for radii and thickness respectively. As with previous projections it is clear that the correlation for radii is stronger than for thickness.

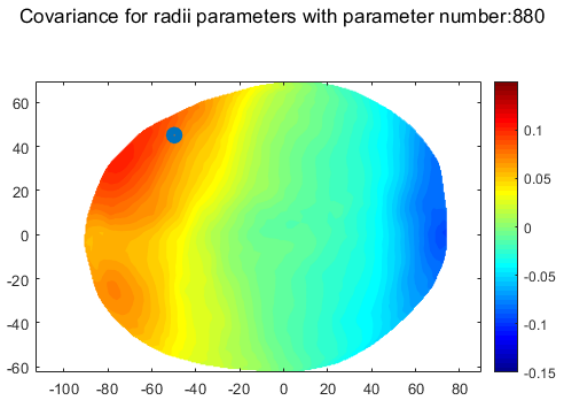

Figure 24: Covariance for thickness parameter number 880 on the side of the forehead (marked with a blue dot), with other radii parameters projected on the skull.

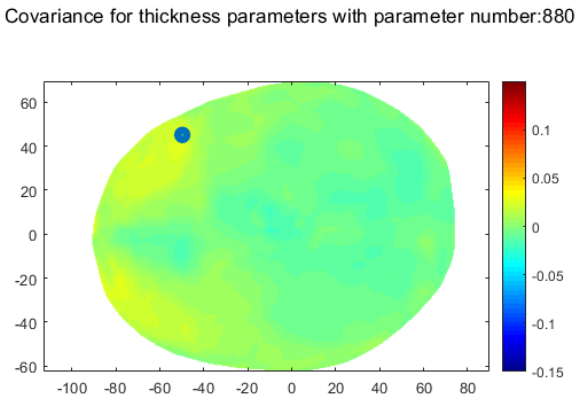

Figure 25: Covariance for thickness parameter number 2990 (marked with a blue dot), with other thickness parameters projected on the skull.

The variance of radii and thickness parameters is shown in Figure 26 and 27. For the radii the parameters varies more at the forehead. For the thickness parameters the variance is the biggest at the place of the sinuses (In Swedish: bihålor) at the skull forehead. Also note the the different scale for each figure.

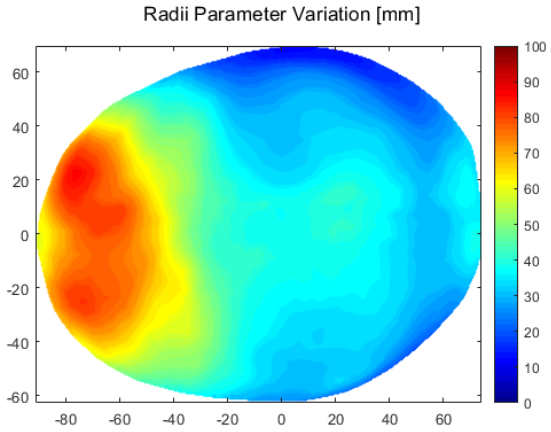

Figure 26: Variation of the radii parameter projected on skull.

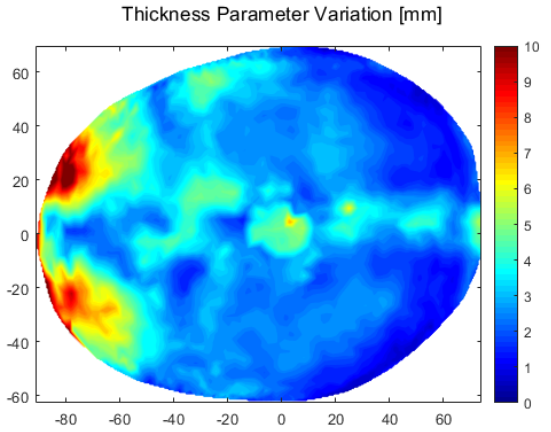

Figure 27: Variation of the thickness parameter projected on skull.

4.2 Parameter Reconstruction

The parameter reconstruction error were an average of 0.95 mm for radii and 1.0 mm for thickness, see Tabular 1. However the reconstruction error varied for each skull. In Figure 28 the average RMS error for each skull is shown.

	Mean RMS Error
Radii	0.9529 ± 0.3422
Thickness	1.0203 ± 0.3236

Table 1: Mean RMS Error for all 29 skulls with 95% standard deviation.

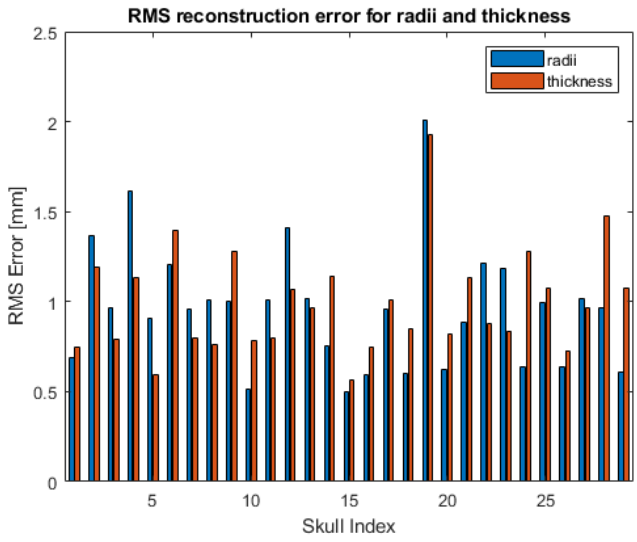

Figure 28: RMS error for all skulls for both radii and thickness.

As seen in Figure 28, skull number 19 were particularly difficult for the shape model to reconstruct and in Figure 29 the residual for all parameters is shown in more detail. This also shows what a typical error residual looks like for a skull.

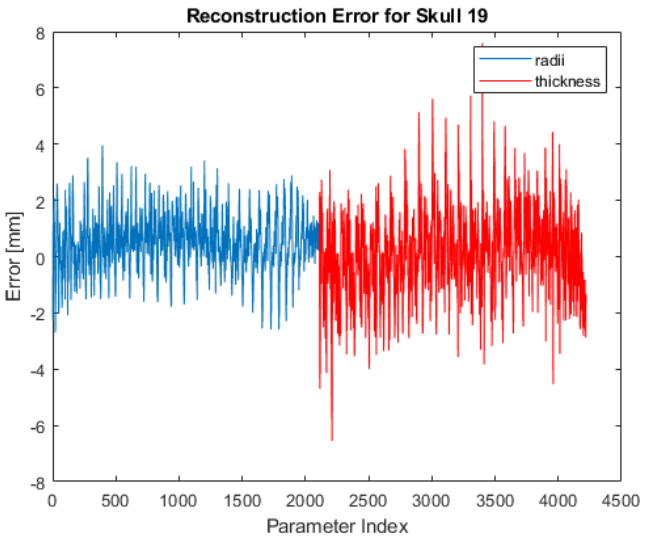

Figure 29: Reconstruction error for skull 19, the skull with highest average reconstruction error.

Taking a look at the reconstructed error projected on the skull number 1 in Figure 30 and 31 we can note the error for thickness is more noisy than for radii. While some parts of the skull is reconstructed quite successfully, there are some parts which the shape models fails to reconstruct properly and these parts are as well more noisy for the thickness parameters.

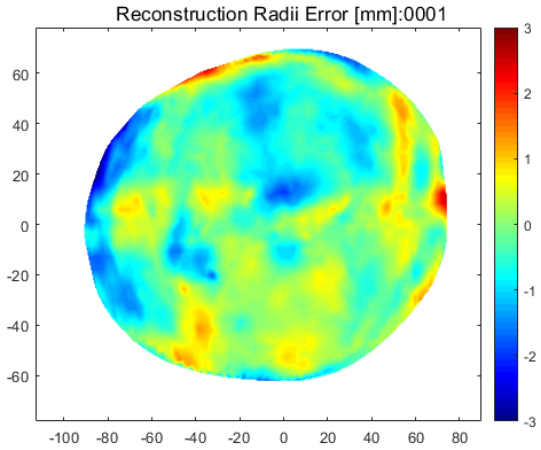

Figure 30: Top view of skull number 1, with the reconstructing error for radii parameters projected on the skull.

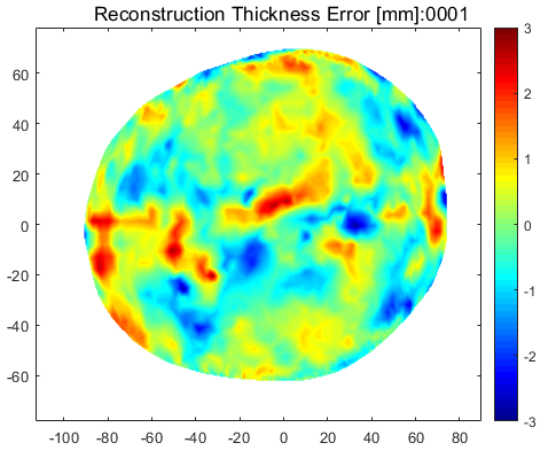

Figure 31: Top view of skull number 1, with the reconstructing error for thickness parameters projected on the skull.

The mean absolute reconstruction error for all skulls is shown in Figure 32 and 33. For radii the mean absolute error is bigger in the front of the skull, for thickness the error is the biggest near the centre line of the skull.

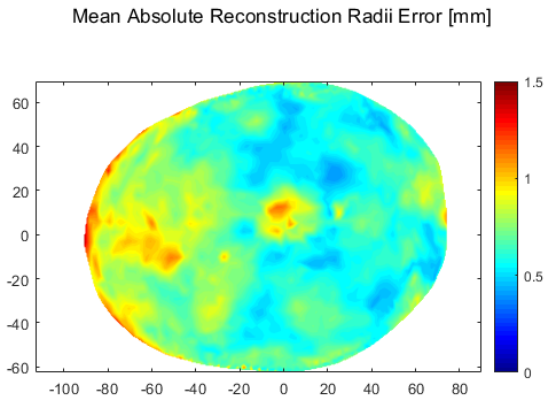

Figure 32: Mean absolute reconstruction error for radii projection on skull.

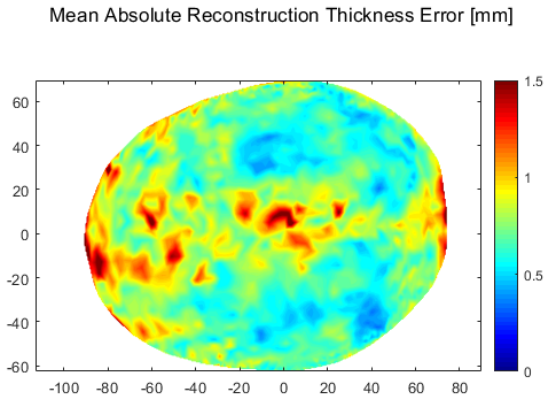

Figure 33: Mean absolute reconstruction error for radii projection on skull.

5 Discussion

A method for reconstructing the skull with an average error of 1 mm has successfully been done. From a collected experience of examples within this study, application on real world cases and 3D printing selected cases, although the average error is 1 mm there is a possibility of a reconstruction produced with an error of up to 5 mm, which is too large to be clinically useful. A 5 mm gap in the border would be easily palpable by the patient by just feeling on the their own skull. Instead to have a reliable method one has to consider the biggest errors on any skull in the data set. This strongly points to that the number of skulls in the data set is too small.

The results showed that there were a lot more correlation for the radii parameters than for the thickness parameters. This probably has to do with that the radii parameters were affected by the chosen method for cropping of the skull, choosing skull centre, sampling of skull. The correlation that so clearly can be seen in Figure 20 and Figure 21 is thus of a nature implying little of the actual skull shape, even though the information of that kind surely is available in the covariance matrix, it cannot be seen in the figures shown but is instead drowned by other information.

Another result probable because of alignment error is the negative correlation we can see with thickness parameters at the sinuses with the back of the head, figure 23. When the head is tilted backwards or forward it moves the sinuses and changes which parameter index the sinuses belongs to. This is believed to be the cause of the negative correlation as seen in the figure.

The average reconstruction error in millimetre was slightly higher for thickness than radii, Tabular 1. This was the case even though the variation for radii was higher than thickness, Figure 26 and Figure 27. As discussed previously the correlation for the radii parameters were high but biased because of probable aligning error. We can draw the conclusion that the shape model can compensate for this bias since the resulting error for radii is smaller than for thickness.

The mean absolute error for radii seen in Figure 32 shows that the biggest reconstruction error is retrieved at the forehead of the skull. If we compare this with the parameter variation shown in Figure 26 we can see this coincides somewhat with where the parameter variation is the largest. For the thickness of the skull, the biggest variation were around the sinuses of the skull, however this the shape model is able to reconstruct quite successfully, instead most of the error is along the centre line of the skull. This also coincides where there is a lot of variation for the thickness parameters of the skull, next to the sinuses at the forehead. We can draw the conclusion that while higher variation for parameters doesn't necessary imply that there will be a higher reconstruction error, it is one of the factors that may cause the error to increase. The reconstruction error projection plots shows an overall noisy result. This is probably

because of the lack of a bigger data set.

In figure 25, which shows how thickness on the side of the skulls is correlated with thickness on other parts of the skull one can see that there is correlation between the thickness on both sides of the skull. This was expected because of the symmetry in the human skull. This can be compared to the symmetry along the middle part of the skull seen in figures 22 and 23.

5.1 Future Work

The cropping of the skull and the subsequent registration of points were two steps in the procedure that could probably be improved. They both impact the end result and while the shape model can to some extend compensate for this, it is believed it cannot to it fully. The cropping should be improved so that it is not simply a transversal crop, this is too much affected by how the patient have been placed during the scanning procedure. Another issue is that no cut by a plane will remove all non desired parts without removing parts of the skull that should be part of the model. A whole different approach for cropping is therefor proposed, perhaps a the cooperation of a radiologist as well as other tools is needed. Another aspect of the project that could have been improved is to use a bigger data set to capture a bigger shape variability among skulls.

In this report we discussed using a more traditional statistical method to model the skull shape. It would however also be interesting to see what the a modern AI based approach could accomplish. For such a method, the preprocessing and parameterization in this report could still be used. The focus could be on building another method for parameter reconstruction that doesn't use PCA. One advantage with such a method is that it could be better at catching nonlinear relationships. [4]

References

[1] Murty, Om. (2009). Variability in thickness of skull bones and sternum. Journal of Forensic Medicine and Toxicology ISSN 0971-1929. https://www.researchgate.net/publication/260944827

[2] Michel A.Audette, Frank P.Ferrie, Terry M.Peters (2000). An algorithmic overview of surface registration techniques for medical imaging, https://www.sciencedirect.com/science/article/pii/S1361841500000141

[3] D. Lacko, T. Huysmans, T. Parizel, G. De Bruyne, S. Verwulgen, M. Van Hulle en J. Sijbers, Evaluation of an anthropometric Shape Model of the Human Scalp, Applied Ergonomics, vol. 48, pp. 70-85, 2015, https://www.researchgate.net/publication/270686799

[4] Zhang, Z. Iterative point matching for registration of free-form curves and surfaces. Int J Comput Vision 13, 119–152 (1994). https://doi.org/10.1007/BF01427149 https://link.springer.com/article/10.1007%2FBF01427149

[5] Karamizadeh, Sasan & Abdullah, Shahidan & Manaf, Azizah & Zamani, Mazdak & Hooman, Alireza. (2013). An Overview of Principal Component Analysis. Journal of Signal and Information Processing. 10.4236/jsip.2013.43B031.

[6] Heimann, Tobias Meinzer, Hans-Peter. (2009). Statistical shape models for 3D medical image segmentation: A review. Medical image analysis. 13. 543-63. 10.1016/j.media.2009.05.004.

[7] Fuessinger, M.A., Schwarz, S., Cornelius, C. et al. Planning of skull reconstruction based on a statistical shape model combined with geometric morphometrics. Int J CARS 13, 519–529 (2018).

[8] Sundseth, Jarle Berg-Johnsen, Jon. (2013). Prefabricated Patient-Matched Cranial Implants for Reconstruction of Large Skull Defects. Journal of central nervous system disease. 5. 19-24. 10.4137/JCNSD.S11106.

[9] Kung W-M, Chen S-T, Lin C-H, Lu Y-M, Chen T-H, Lin M-S (2013) Verifying Three-Dimensional Skull Model Reconstruction Using Cranial Index of Symmetry. PLoS ONE 8(10): e74267. https://doi.org/10.1371/journal.pone.0074267

[10] The Cancer Imaging Archive (TCIA), 2019 https://www.cancerimagingarchive.net/

Master's Theses in Mathematical Sciences 2020:E37
ISSN 1404-6342

LUTFMA-3417-2020

Mathematics
Centre for Mathematical Sciences
Lund University
Box 118, SE-221 00 Lund, Sweden

http://www.maths.lth.se/